Crystal Structure of the C-Terminal Half of Tropomodulin and Structural Basis of Actin Filament Pointed-End Capping

Inna Krieger,*† Alla Kostyukova,* Atsuko Yamashita,* Yasushi Nitanai,* and Yuichiro Maéda*
*Laboratory for Structural Biochemistry, RIKEN Harima Institute at SPring-8, Hyogo, Japan 679-5148; and †GosNII Genetika, Protein Chemistry Laboratory, Moscow 113545, Russia

ABSTRACT Tropomodulin is the unique pointed-end capping protein of the actin-tropomyosin filament. By blocking elongation and depolymerization, tropomodulin regulates the architecture and the dynamics of the filament. Here we report the crystal structure at 1.45-Å resolution of the C-terminal half of tropomodulin (C20), the actin-binding moiety of tropomodulin. C20 is a leucine-rich repeat domain, and this is the first actin-associated protein with a leucine-rich repeat. Binding assays suggested that C20 also interacts with the N-terminal fragment, M1-M2-M3, of nebulin. Based on the crystal structure, we propose a model for C20 docking to the actin subunit at the pointed end. Although speculative, the model is consistent with the idea that a tropomodulin molecule competes with an actin subunit for a pointed end. The model also suggests that interactions with tropomyosin, actin, and nebulin are all possible sources of influences on the dynamic properties of pointed-end capping by tropomodulin.

INTRODUCTION

The actin filament plays essential roles in a variety of biological functions, such as muscle contraction, calcium regulation, organelle transportation, and cell division, among others. The actin filament is polar, so that the barbed end is distinct from the pointed end in its structure as well as in its dynamic properties. Tropomodulin (~40 kDa) specifically binds to the pointed end of the actin-tropomyosin filament and thereby alters the dynamic properties of the pointed end and specifies the filament length. Capping by tropomodulin is not static, but dynamic (Littlefield et al., 2001; Littlefield and Fowler 1998; Weber et al., 1999); in vivo the pointed end is transiently capped by tropomodulin so that the actin subunits as well as tropomodulin itself at the pointed ends are exchanged with free molecules in the pool. It is also postulated that the capping by tropomodulin is regulated by the conformation of the actin-tropomyosin filament. Tropomodulin is distributed over a wide variety of mammalian cells, and so far four types of tropomodulin isoforms have been distinguished (Conley et al., 2001; Cox and Zoghbi, 2000). A homolog (*Sanpodo* gene product) in *Drosophila* is known to be responsible for the asymmetric division of nervous cells (Park et al., 1998).

At the pointed ends, tropomodulin interacts with actin, tropomyosin, and if present, nebulin. The affinity of tropomodulin for the pointed end of the actin filament in the absence of tropomyosin is low ($K_d \approx 0.3–0.4\ \mu M$), whereas in its presence the affinity is higher by a factor of more than 1000 ($K_d \approx 50$ pM) (Weber et al., 1999). It has been suggested that the C-terminal half of tropomodulin is responsible for the interaction with actin (Gregorio et al., 1995), whereas the N-terminal half of tropomodulin interacts with tropomyosin (Babcock and Fowler, 1994; Fowler, 1990; Vera et al., 2000), although no details are known about either interaction. Tropomyosin is a rod-like, α-helical coiled coil protein that associates in a head-to-tail manner, forming a strand. The tropomyosin strands lie on the surface of the actin filament with the N-terminus toward the pointed end. Nebulin is a giant protein (molecular mass, 800 kDa), which is supposed to be a molecular ruler for determining the thin filament length (Labeit and Kolmerer, 1995). It is mainly composed of repeating modules that are ~35 amino acid residues long. The molecule forms an α-helix in an acidic environment, and it is likely to extend all along the thin filament of vertebrate skeletal muscle (Labeit and Kolmerer, 1995; Pfuhl et al., 1994, 1996), but not cardiac muscle, with its N-terminus toward the pointed end. The N-terminal part of nebulin consists of N-term, the 77-residue-long N-terminal-specific segment, followed by M1-M2-M3 (amino acid residues 78–185), consisting of three repeating modules. Tropomodulin interacts more strongly with the fragment M1-M2-M3 than with N-term-M1-M2-M3 (McElhinny et al., 2001). It is not known whether nebulin promotes an increase in the tropomodulin affinity for the pointed ends, as tropomyosin does.

To understand the mechanism of the pointed-end capping with tropomodulin, structural information is essential. Until we analyzed the x-ray solution scattering profiles recently (Fujisawa et al., 2001), even the overall shape of the molecule had been controversial. Here we report the crystal

Submitted February 19, 2002, and accepted for publication July 16, 2002.

I. Krieger and A. Kostyukova contributed equally to this work.

I. Krieger's present address: Los Alamos National Laboratory, Los Alamos, NM 87545.

A. Kostyukova's present address: Department of Neurology and Cell Biology, UMDNJ-RWJMS, 675 Hoes Lane, Piscataway, NJ 08854.

Address reprint requests to Dr. Yuichiro Maéda, RIKEN Harima Institute at SPring-8, Mikazuki, Sayo, Hyogo 679-5148, Japan. Tel.: 81-791-582822; Fax: 81-791-582836; E-mail: ymaeda@spring8.or.jp.

The atomic coordinates and structure factors have been deposited in the Protein Data Bank, www.rcsb.org (PDB code 1IO0).

0006-3495/02/11/2716/10 $2.00

structure of the C-terminal half of tropomodulin. The C-terminal half was chosen as the first target for the crystallographic study, partly because this part is of primary importance in the tropomodulin-actin interaction and partly because of its compact structure, as our previous results had indicated (Fujisawa et al., 2001; Kostyukova et al., 2000, 2001). This protein consists of two halves, the N-terminal half and the C-terminal half, which are functionally as well as structurally distinct from each other (Fujisawa et al., 2001; Kostyukova et al., 2000, 2001). The N-terminal half is elongated and flexible and has no definite tertiary structure in solution, but it becomes structured upon binding to tropomyosin. On the other hand, the C-terminal half represents a compact and tightly folded domain, which thermally melts as a unit through a two-state transition.

The crystal structure indicates that the C-terminal half of tropomodulin (C20) is a leucine-rich repeat (LRR) domain (Buchanan and Gay, 1996; Kobe and Deisenhofer 1994, 1995a; Kobe and Kajava, 2001). This is the first actin-associated protein with an LRR motif. In many proteins of diverse origin, function, and cellular location, the LRR domains are involved in protein-protein interactions, and thus we tested whether C20 interacts with tropomyosin and nebulin. Based upon the atomic structure and the results of binding assays, we propose a model for the molecular arrangement at the pointed end, which will serve as the framework for future investigations on protein-protein interactions and the mechanism of pointed-end capping.

MATERIALS AND METHODS

Protein preparations

A variant of chicken E-tropomodulin, designated as Tmod (N39), was overexpressed in and purified from *Escherichia coli* as previously described (Kostyukova et al., 2000). Tmod (N39) has an extra His-tag (6 His residues) at the N-terminus and lacks 15 residues at the C-terminus. The C-terminal half of tropomodulin, C20 (amino acids 160–344), was prepared by the limited proteolysis of Tmod (N39) with *Streptococcus aureus* V8 protease, followed by anion-exchange chromatography (Kostyukova et al., 2000). The nebulin M1-M2-M3 fragment was prepared by overexpression in *E. coli* using the plasmid that was kindly provided by Dr. C. C. Gregorio (McElhinny et al., 2001). Tropomyosin was obtained from bovine heart, by using the procedures described previously (Miegel et al., 1992). Troponin C of rabbit skeletal muscle origin was expressed in and purified from *E. coli*, as previously described (Fujita-Becker et al., 1993).

Crystallization and data collection

Crystals of C20 were grown using the vapor diffusion method at 22°C, as previously described (Krieger et al., 2001). Briefly, the protein solution (4 μl of 10 mg/ml C20 in 25 mM glycine buffer, pH 3.0) was mixed with 2 μl of precipitating solution. The precipitating solution was composed of 0.1 M MES-NaOH buffer, pH 6.5, 24% v/v PEG 400, and 10 mM $ZnSO_4$, whereas the reservoir solution contained 0.1 M MES-NaOH buffer, pH 6.5, 15% v/v PEG 400, and 6 mM $ZnSO_4$ (Krieger et al., 2001). Before collecting the x-ray diffraction data, the crystals were cryoprotected by adding glycerol to a final concentration of 25% in the mother liquor, mounted on cryoloops, and flash frozen in liquid nitrogen. All of the x-ray diffraction data were collected from frozen crystals (90 K) at the beam-line BL44B2 of SPring-8, with a Mar-CCD165 detector. The data were processed using the DENZO and SCALEPACK programs from the HKL2000 package (Otwinowski, 1997). Statistics are summarized in Table 1.

Structure determination and refinement

The structure was solved by the multi-wavelength anomalous dispersion (MAD) method using Zn^{2+} incorporated into the native crystals during crystallization. Heavy atom position searching and phase calculations up to 1.8 Å were undertaken with the program SOLVE (Terwilliger and Berendzen, 1999). The initial phases were improved by density modification, using solvent flattening and histogram matching by DM (CCP4, 1994). At this stage the WarpNtrace procedure of ARP/wARP (Perrakis et al., 1999) was used to attempt automatic model tracing. ARP/wARP was able to automatically build 158 of 185 residues in two continuous main-chain fragments. Manual fitting and tracing were undertaken using TURBO-FRODO (Roussel and Cambillau, 1996). ARP was used to add water molecules automatically. A high-resolution data set with the resolution extended to 1.45 Å was used in the model refinement. The model was refined by REFMAC (CCP4, 1994) and by XPLOR 3.851 (Brünger, 1992).

Binding experiments

For the blot overlay experiments, Tmod (N39) and C20 were biotinylated with biotinamidocaproate-*N*-hydroxysulfosuccinimide ester (BAC-SulfoNHS) according to the manufacturer's instructions (Sigma Chemical Co., St. Louis, MO). The nebulin fragment, together with tropomyosin and troponin C as controls, were applied as dots on nitrocellulose filters and were incubated after blocking with 0.4 mg/ml biotinylated proteins in PBS buffer (0.01 M phosphate buffer, 0.138 M NaCl, 2.7 mM KCl, pH 7.4) for 30 min. Binding of the biotinylated proteins was detected with ExtrAvidin peroxidase according to the manufacturer's instructions (Sigma).

RESULTS AND DISCUSSION

Overall structure

We crystallized the tropomodulin fragment C20, a fragment with a chain weight of ~20 kDa spanning amino acid residues 160–344, of chicken E-tropomodulin. This fragment includes almost the entire C-terminal half of the molecule, lacking 15 residues at the original C-terminus (Kostyukova et al., 2000). Attempts to crystallize full-length tropomodulin have been unsuccessful. The crystal structure of C20 (Fig. 1) was determined at 1.45-Å resolution, using the multi-wavelength anomalous dispersion method on the native crystal with Zn^{2+}, which was introduced in the process of crystallization. The refined C20 model has a crystallographic R value of 0.203 and a free R value of 0.220. The structure determination and the model refinement statistics are summarized in Table 1. The first N-terminal 19 residues, Gly160–Pro178, do not give any clear electron density, and these are likely to be flexible and disordered.

C20 folds into a typical LRR domain (for review see Buchanan and Gay, 1996; Kobe and Deisenhofer, 1994, 1995a; Kobe and Kajava, 2001); C20 consists of five tandem repeats of a 28–30-residue-long, homologous α/β

TABLE 1 X-ray structure determination and refinement statistics

	Data collection: space group $R3$; unit-cell parameters $a = b = 69.29$ Å, $c = 101.23$ Å, $\alpha = \beta = 90°$, and $\gamma = 120°$						Mean figure of merit	
	Wavelength (Å)	Resolution (Å)	Number of reflections/unique	Redundancy	Completeness (%)*	*R*-merge*†	MAD phasing	Density modification
Zn-peak	1.2836	20-1.8	143,600/16,745	8.6	99.9 (100)	0.045 (0.082)		
Zn-edge	1.2841	20-1.8	143,829/16,777	8.6	99.9 (100)	0.045 (0.083)	0.710	0.878
Zn-remote	1.2800	20-1.8	143,705/16,753	8.6	99.9 (100)	0.051 (0.093)		
High resolution§	0.7	20-1.45	357,913/31,954	11.2	100 (100)	0.076 (0.286)		
Refinement statistics Resolution = 10.0-1.45 Å R_{cryst}/R_{free} = 0.203/0.220‡ Average isotropic B value = 18.9 Å^2 Number of protein atoms = 1297 Number of Zn atoms = 1 Number of water molecules = 231 RMSD bond length = 0.005 Å RMSD bond angles = 1.052°								

*Values for the last resolution shell (1.86-1.80 Å for Zn-MAD data sets and 1.50-1.45 Å for high-resolution data set) are in parentheses.
†*R*-merge = $\Sigma_h\Sigma_I|I_{h,I} - \langle I\rangle_h|/\Sigma|\langle I\rangle_h|$.
‡R_{cryst}, crystallographic *R*-factor calculated on 95% of all data in the resolution range, used in the model refinement; R_{free}, *R*-factor calculated for randomly selected 5% of all data omitted in the model-building and refinement process.
§Two data sets with 1- and 20-s exposure times for low- and high-resolution diffraction measurements were merged by SCALEPACK (Otwinowski, 1997).

structural unit (Fig. 2), followed by a nonhomologous α6 helix at the C-terminus. The five repeats form a continuous right-handed super-helix of alternating α-helices and β-strands, resembling a horseshoe of ~45 Å width × 30 Å length × 20 Å thickness (Fig. 1, *a* and *b*). The additional helix α6 protrudes from the horseshoe with 2.5 turns of ~16 Å. This C20 structure is consistent with the molecular envelope obtained by the small-angle x-ray scattering (Fujisawa et al., 2001). The tight and compact folding of this protein also explains well the cooperative and single-step melting property of the protein, revealed by differential scanning calorimetry (Kostyukova et al., 2001).

Despite the structural similarities among the five LRRs of C20, each LRR slightly differs in its folding. First, the repeat length is varied by insertions in its connecting loop. Repeat 1 has two one-residue insertions, in both the $\alpha\beta$-loop connecting α1 to β1 and the $\beta\alpha$-loop connecting β1 to α2, whereas repeat 4 has a two-residue insertion in its $\beta\alpha$-loop. It is interesting to note that the sequences of these extended loops are strongly dependent on the isoform types (Fig. 2). Second, at either end of the LRRs, repeats 1 and 5 have some irregularities. Repeat 1 has a shorter α-helix, with three turns instead of four, whereas repeat 5 has a shorter loop downstream of β5.

On the horseshoe, four surfaces are distinguished (Figs. 1, *a* and *b*, and 2): α-, $\alpha\beta$-, β-, and $\beta\alpha$-surfaces. The α-surface forms the outer circumference where five parallel α-helices are aligned, whereas the β-surface is on the inner surface of the horseshoe, lined with five parallel β-strands (Fig. 1 *c*). The $\alpha\beta$-surface and the $\beta\alpha$-surface are formed by the $\alpha\beta$-loops and the $\beta\alpha$-loops, respectively, and the α6-helix projects from the $\alpha\beta$-surface like an arm. It is worth noting that Asn179, which is the first N-terminal residue recognized clearly in the electron density map, is located in the vicinity of the $\beta\alpha$-surface (Fig. 1 *b*).

Electrostatic potentials on the surfaces (Fig. 3, *a* and *b*) reveal the remarkable asymmetric localization of electric charges; the α-surface is predominantly negatively charged, whereas the large area extending from the β-surface to the $\alpha\beta$-surface is positively charged. The positively charged area includes the basic residues of Lys227, Lys228, Arg286, Lys255, and Lys314, which are conserved or equivalently substituted among the isoforms, except for Lys255 (Figs. 2 and 3 *c*). Furthermore, the arm of α6 proximal to the area is also positively charged, because it has four contiguous basic residues near the C-terminus: Arg340-Lys341-Arg342-Arg343. This cationic nature is highly conserved among the isoforms (Fig. 2). From the standpoint of the locations of hydrophobic residues, the arm of α6 is also remarkable because of its hydrophobic armpit, formed by Ile283, Leu313, Leu338, and Val339, which are exposed to the solvent and highly conserved, except for Ile283 (Figs. 2 and 3 *c*). Therefore, α6 is characterized not only by its protruding geometry but also by its surface properties.

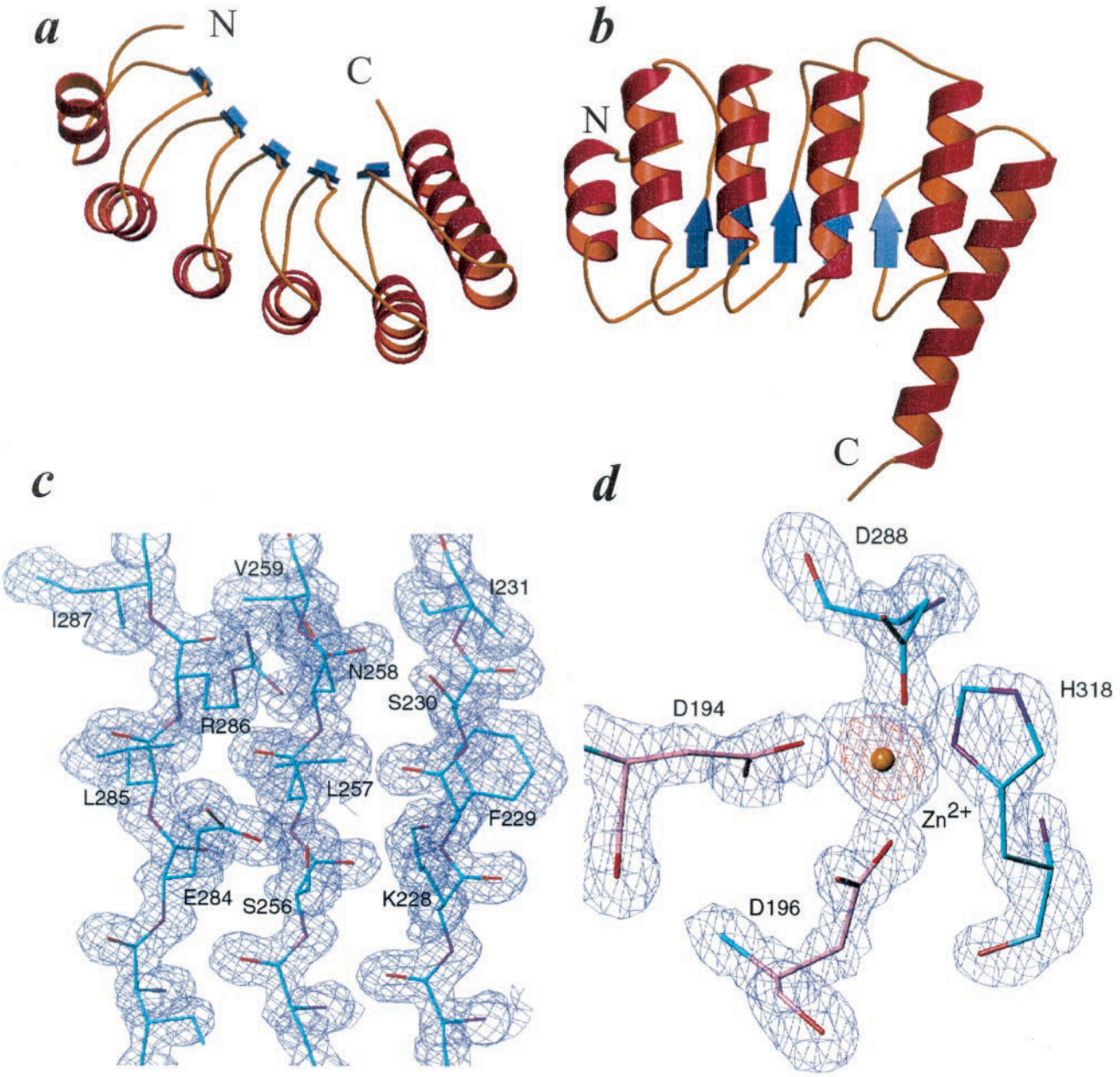

FIGURE 1 The atomic structure of the C-terminal half of tropomodulin (C20). (*a* and *b*) The ribbon model of C20, viewed from the $\beta\alpha$-surface and the α-surface, respectively; (*c*) A part of the β-surface, indicated as the final $|2F_o - F_c|$ electron density map at 1.45-Å resolution (contoured at 1 σ); (*d*) The region around Zn^{2+}, which is coordinated between two adjacent molecules, shown in cyan and purple, with the final $|F_o - F_c|$ electron density map. The map was calculated with the phases from the model, except for the zinc atom and the coordinating residues (D194, D196, D288, and H318). Contour levels of maps in deep blue and red are 4 σ and 15 σ, respectively. *a* and *b* were generated with MOLSCRIPT (Kraulis, 1991) and RASTER3D (Meritt and Murphy, 1994), and *c* and *d* were generated with TURBO-FRODO (Roussel and Cambillau, 1996).

C20 was crystallized only in the presence of Zn^{2+} ions (Krieger et al., 2001). In the crystal structure, a Zn^{2+} is tetragonally coordinated by Asp194 and Asp196 of one molecule and Asp288 and His 318 of the adjacent molecule in the crystal lattice (Figs. 1 *d* and 2). It is not known whether this protein in vivo binds Zn^{2+} and whether this protein is regulated by cation binding. Some other proteins are known to bind nonphysiological Zn^{2+} and/or Cd^{2+} on the surface of the proteins, improving the crystal quality (Trakhanov et al., 1998; Trakhanov and Quiocho, 1995).

Structural features characteristic of C20 but not of other LRR proteins

Tropomodulin had been proposed to have the LRR motif by PSI-BLAST (Altschul et al., 1997) searches, due either to its

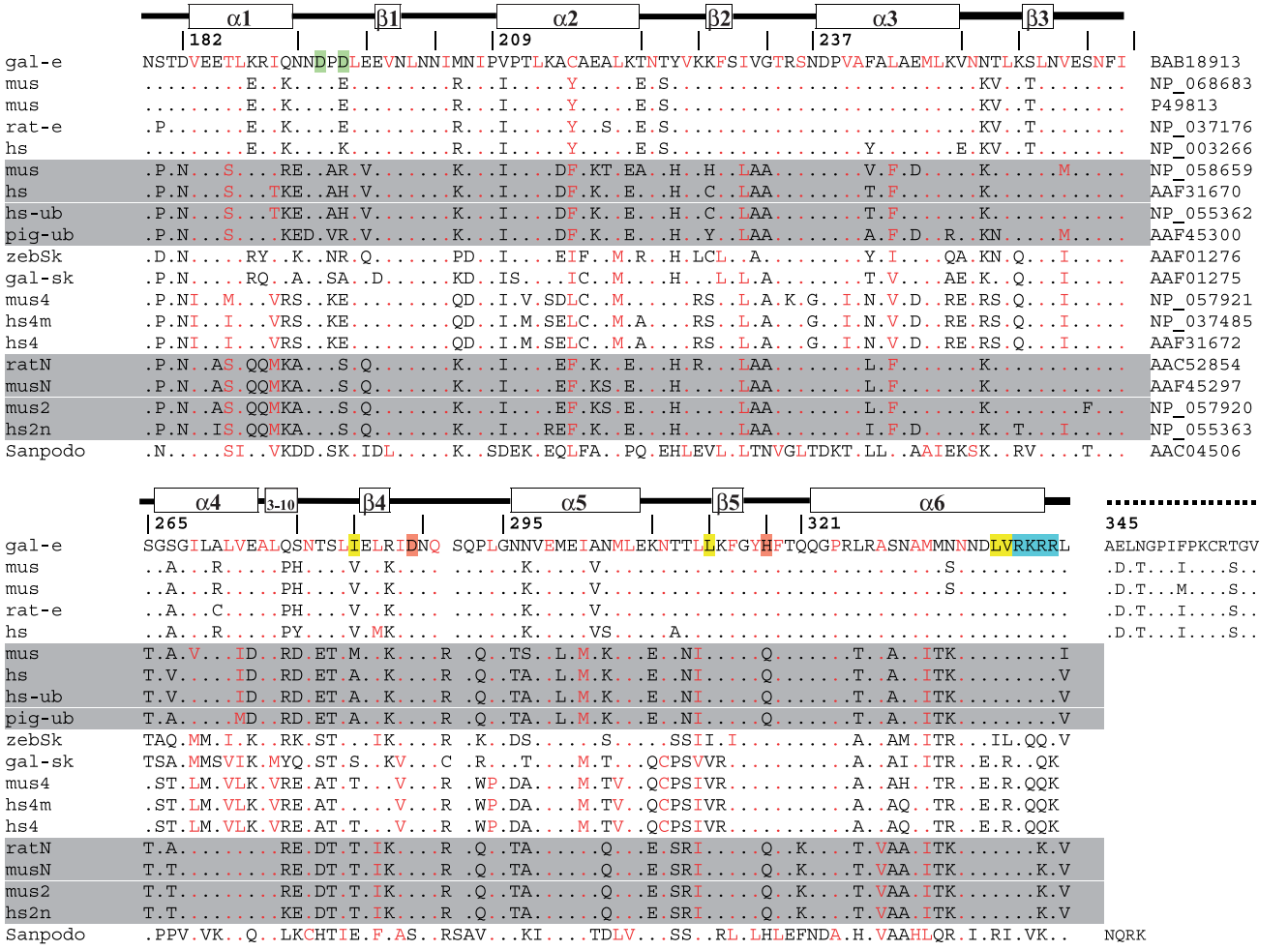

FIGURE 2 The amino acid sequence and the secondary structure. The amino acid sequences of four types of tropomodulin isoforms from vertebrates, together with the *Sanpodo* gene product, the tropomodulin homolog from *Drosophila melanogaster*, are aligned to the chicken E-type tropomodulin sequence on the top. The amino acid residues from Asn-179 to Leu-344 have electron densities in the crystal structure reported here, whereas Arg-345 and the subsequent residues, indicated by a broken line, were removed during the protein preparation. The isoform types are, from top to bottom, E-type, U(ubiquitous)-type, Sk-type, N(neural or brain)-type, and Sanpodo. The accession number for each sequence is given at the end of each line in the top half of the panel. Above the chicken E-type tropomodulin sequence, the boundaries between four surfaces of the LRR domain (α-, $\alpha\beta$-, β-, and $\beta\alpha$-surfaces) are indicated by the vertical bars, whereas the boundaries of the secondary structures (α for α-helix, β for β-strand, and 3–10 for helix 3–10) are indicated by boxes. Boxes are connected by solid lines, indicating loops. The helix α6 is not a part of the LRRs. In the sequences on the second line and below, residues identical to the sequence of the top line are indicated by dots, whereas nonidentical residues are indicated by one-letter symbols. Residues in red are buried, forming the core of the molecule. Residues highlighted in green (Asp194 and Asp196) and in red (Asp288 and His318) are coordinated to Zn^{2+}. Residues highlighted in yellow (Ile283, Leu313, Leu338, and Val339) are those forming the hydrophobic pit, whereas residues highlighted in blue (Arg340, Lys341, Arg342, and Arg343) are the positively charged four contiguous residues.

similarity to the myosin-I-binding protein Acan125 (Xu et al., 1997) or to pig RNase inhibitor (A. G. Murzin, MRC Centre for Protein Engineering, Cambridge, U.K., personal communications). Despite the fact that C20 shares the overall folding topology with other LRR proteins, especially with those containing a 28-residue repeat, like the RNase inhibitor (Kajava, 1998), C20 has characteristic features in its loop regions. The $\beta\alpha$-loops of C20 have large side chains that protrude from the middle of the $\beta\alpha$-surface, forming an extended ridge. This is characteristic of C20 but not of the structure of the RNase inhibitor. The $\alpha\beta$-surface of C20 is characterized by asparagine residues at the beginning of the $\alpha\beta$-loops of repeats 2–5 (Asn223, Asn251, Asn279, and Asn309, respectively), which form hydrogen bonds with adjacent loops as well as with the main chain downstream within the same repeat. This hydrogen bond network resembles those formed by the asparagine ladder (Kobe and Deisenhofer, 1995a) often occurring in the $\beta\alpha$-loops of other LRR proteins, although between the two, there are some differences in the manner of hydrogen bonds. To our knowledge, this is the first structure of a LRR domain with an asparagine ladder in the $\alpha\beta$-loops. In a recent review

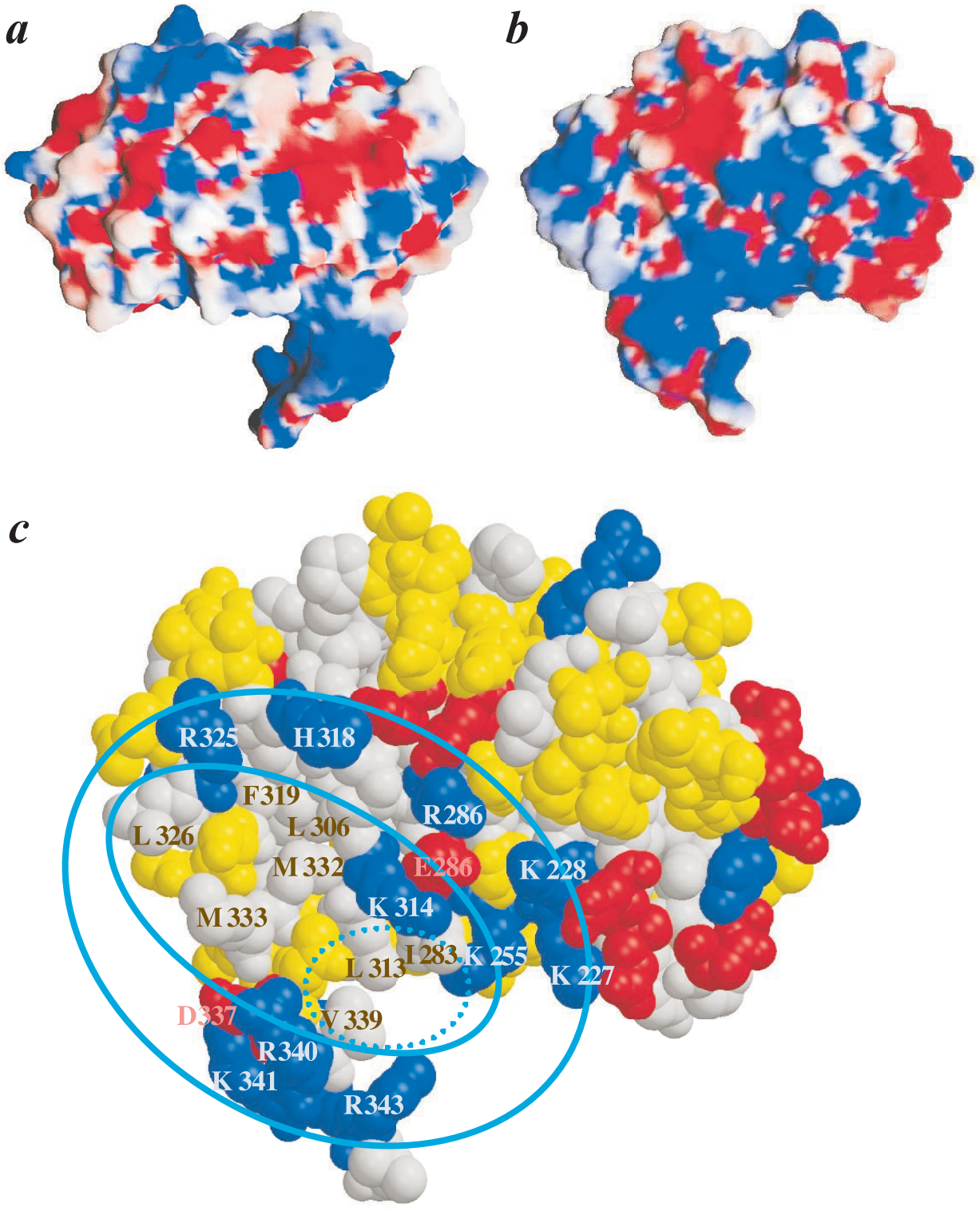

FIGURE 3 (*a* and *b*) The electrostatic surface potential of C20 calculated by the Poisson-Boltzmann method, assuming dielectric constants of 2 and 80 for the interior of C20 and the solvent region, respectively, and 0.1 M for the salt concentration. The molecular surfaces are colored according to the electrostatic potential, so that colors from red to blue indicate the potential from negative to positive. (*a*) α-surface; (*b*) β-surface; (*c*) CPK representation of the C20 β-surface. Atoms in red are acidic residues (Glu or Asp), those in blue are basic residues (His, Lys, or Arg), atoms in yellow indicate polar residues (Gln, Apn, Ser, Thr, or Tyr), and those in gray indicate nonpolar residues (Gly, Ala, Val, Leu, Ile, Phe, Trp, Pro, Cys, or Met). The dotted circle indicates residues forming the hydrophobic pit, which is surrounded by basic residues indicated between two ellipses. *a* and *b* were created with GRASP (Nicholls et al., 1991), whereas *c* was generated with MOLSCRIPT and RASTER3D.

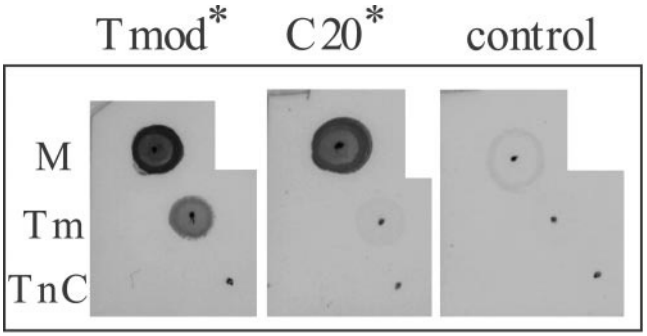

FIGURE 4 Interaction of C20 or Tmod (N39) with nebulin, and tropomyosin, as determined by dot overlay experiments. The nebulin M1-M2-M3 fragment (M), tropomyosin (Tm), and troponin C (TnC) were applied as dots on nitrocellulose filters, as indicated. Left and center panels, marked as Tmod* and C20*, represent incubation with biotinylated Tmod (N39) and biotinylated C20, respectively. Binding of the biotinylated proteins was detected using ExtrAvidin peroxidase (Sigma). The right panel represents the control: a nitrocellulose filter incubated directly with ExtrAvidin peroxidase.

(Kobe and Kajava, 2001), it has been postulated by modeling that the characteristic horseshoe structure of the LRR proteins does not require the presence of an asparagine (or cysteine) ladder at the conventional position, i.e., after the β-sheet. The structure of C20 confirms this notion.

C20 binds to actin and nebulin

Actin polymerization is inhibited by tropomodulin alone, in the absence of tropomyosin, indicating that tropomodulin interacts with actin (Weber et al., 1994). The interaction with actin has been proposed to occur in the C-terminal half of tropomodulin. A monoclonal antibody bound to the C-terminal half prevented tropomodulin from blocking elongation and depolymerization from the pointed ends of gelsolin-capped actin filaments (Gregorio et al., 1995). Recent results indicate that the C-terminal portion of tropomodulin inhibits actin elongation from the pointed ends of gelsolin-capped actin filaments, although to a somewhat lesser extent as compared with intact tropomodulin (V. M. Fowler, Scripps Research Institute, La Jolla, CA, personal communication). These results clearly indicated that the C-terminal half of tropomodulin is responsible for the capping of the pointed end. It has also been known that the N-terminal half of tropomodulin is responsible for the interaction with tropomyosin (Babcock and Fowler, 1994; Fowler, 1990; Vera et al., 2000).

To extend our knowledge about the proteins interacting with the C-terminal half of tropomodulin, we studied the interactions of C20 with an N-terminal nebulin segment M1-M2-M3 by dot overlay experiments. As shown in Fig. 4, Tmod (N39) interacts with nebulin (M1-M2-M3) and tropomyosin, whereas C20 interacts with nebulin (M1-M2-M3) but not with tropomyosin. Troponin C does not interact with either Tmod (N39) or C20, as expected. These results are consistent with and complementary to the previous results of solid-phase binding assays, in that the N-terminal half of tropomodulin binds to tropomyosin (Babcock and Fowler, 1994) and the intact tropomodulin molecule interacts with nebulin fragments (McElhinny et al., 2001). The dot overlay results are consistent with our gluteraldehyde cross-linking experiment (data not shown), in which the formation of a nebulin (M1-M2-M3)-C20 complex was detected.

Altogether, the C-terminal half accommodates binding sites for actin and nebulin, whereas the N-terminal half has the binding site for tropomyosin.

Possible docking model for C20 to the pointed end of the actin filament

Based upon the crystal structure and the binding specificity of C20, we constructed a possible docking model for C20 to the pointed end of the actin-tropomyosin filament. We considered the following points. First, the LRR domain interacts with its target protein through the β-surface in the RNase-RNase inhibitor complex (Kobe and Deisenhofer, 1995b; Papageorgiou et al., 1997) as well as in the U2B"-U2A' complex (Price et al., 1998). Although the complex structures available to date are too few to be generalized, the β-surface of C20 should be the most plausible interface to the polymeric actin (F-actin). Second, the large positively charged area on the β-surface is most likely to interact with F-actin, which has an essentially negatively charged surface (Fig. 5 *a*) except for the hypothetical tropomyosin binding area (Saeki et al., 1996). Third, the missing N-terminal half of tropomodulin should be located so that it is allowed to interact with tropomyosin. Because the N-terminus of C20 is located near the $\beta\alpha$-surface, it is less plausible that the $\beta\alpha$-surface is involved in the interface with F-actin. Fourth, the docking of C20 to the pointed end should be associated with the interaction of C20 with nebulin. Fifth, one tropomodulin molecule is required to block elongation completely from the pointed ends of actin-tropomyosin (Weber et al., 1999).

To narrow down the plausible models to a unique one, we considered the fact that, in the pointed-end capping, tropomodulin competes with actin monomers for the pointed end (see Fig. 1 of the reference Weber et al., 1999). Therefore, we assumed that C20 should mimic the binding of an actin monomer to F-actin (Fig. 5 *b*). This simple idea led us to discover many possible and preferable interactions between C20 and F-actin. 1) The actin helix of Ala181-Glu195 (assigned by 1J6Z (Otterbein et al., 2001)) laid on the surface is highly complementary to the β-surface of C20 (Fig. 5 *c*): actin:Arg183-C20:Glu199, actin:Asp184-C20:Lys227, actin:Asp187-C20:Lys228, actin:Lys191-C20:Glu284, and actin:Glu195-C20:Lys314. These C20 residues are highly conserved among the four isoforms of tropo-

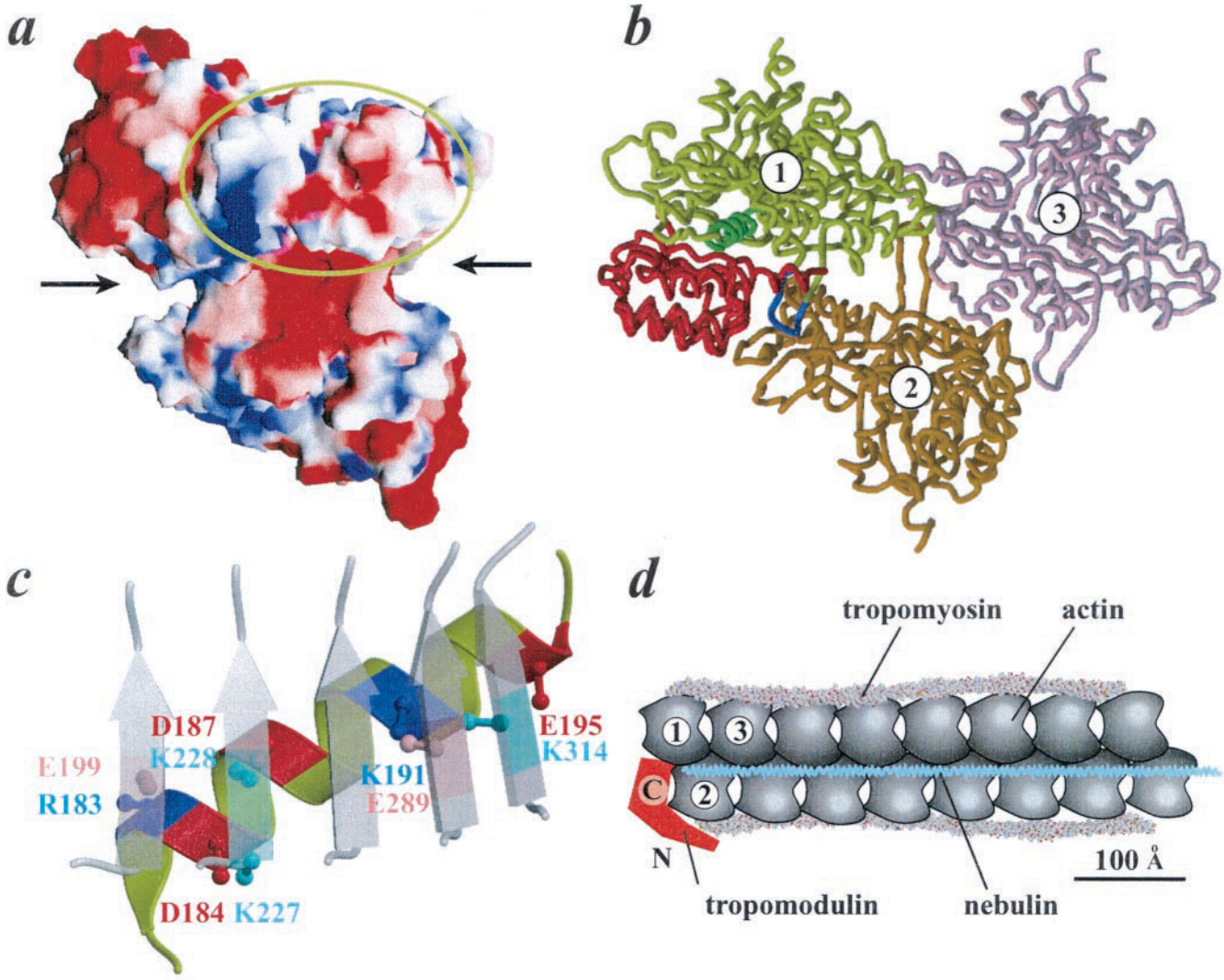

FIGURE 5 Possible interaction of C20 with actin and model for the pointed end of the actin-tropomyosin filament. (*a*) Electrostatic surface potential of the F-actin pointed end. Three actin subunits, aligned in an F-actin model (Lorenz et al., 1993), are viewed from the pointed end along the direction slightly tilted relative to the filament axis. The pointed-end surface of the end actin subunit is highlighted with the yellow circle. The arrows indicate the negatively charged major grooves of the actin filament. (*b*) Proposed docking model for C20 to F-actin, viewed from a direction perpendicular to the filament axis. Each molecule is indicated by the C_α backbone, and three actin subunits (in yellow, orange, and magenta) from the pointed end are numbered, whereas C20 is indicated in red. The α-helix of actin subunit 1 and the hydrophobic plug of subunit 2, which are involved in the interface to C20 in this model, are indicated in green and blue, respectively. Note that α6 is positioned at the entrance of the major groove of F-actin. (*c*) Interface formed between the β-surface of C20 and the α-helix of actin subunit 1 (as indicated in *b*), viewed out from C20. The β-strands of C20 and the helix of the actin are indicated in translucent gray and yellow, respectively. Positively charged residues of C20 and the actin are colored sky blue and blue, respectively, and negatively charged residues of C20 and the actin are colored pink and red, respectively. Ball-and-stick models show the C_α and C_β positions of these residues. (*d*) Model for the pointed end with actin, tropomyosin, tropomodulin, and nebulin. As in *b*, three actin subunits from the pointed end are numbered, and the tropomodulin is indicated in orange, consisting of the N-terminal half (N) and the C-terminal half (C). The overall helical twist is omitted for clarity. Tropomyosin molecules are indicated according to the model coordinates by Dr. Haruki Nakamura (Osaka University). *a* was generated by GRASP, and *b* and *c* were generated with MOLSCRIPT and RASTER3D.

modulin (Fig. 2). 2) This docking results in placing the tip of the α6-helix at the entrance to the major groove of the actin filament. The C-terminal end of α6 is highly positively charged, whereas the inside wall of this groove is highly negatively charged (Fig. 5 *a*). It is interesting to note that a model has been proposed in which two nebulin molecules occupy symmetrical positions along the major grooves of the actin filament (Labeit and Kolmerer, 1995; Pfuhl et al., 1994, 1996), although we do not know at present any details about the interaction of actin and C20 to the N-terminal portion of nebulin (see also Lukoyanova et al., 2002). 3) The hydrophobic armpit of α6 is located in the proximity of the actin loop spanning from Gln263 to Phe270, which includes Phe266 and Ile267 at its tip. Although the crystal

structure of monomeric actin (Kabsch et al., 1990; Otterbein et al., 2001) shows the loop lying down on the actin surface, upon docking with C20, conformational changes of the loop would enable Phe266 and/or Ile267 to plug into the pit, forming a hydrophobic core (Holmes et al., 1990).

A model for the pointed end of the actin-tropomyosin filament

Based on our crystal structure, the docking model, and previous results by others, we propose a model for the arrangement of protein molecules at the pointed end of the actin-tropomyosin filament (Fig. 5 *d*). At the pointed end, a tropomodulin molecule is anchored on one hand to the tropomyosin strand and on the other to the nebulin strand, with the interface to actin in between, occupying the position for the next actin subunit. In solution, tropomodulin is an elongated molecule ~115 Å long (Fujisawa et al., 2001). Upon binding to the pointed end of the filament, the tropomodulin may kink, presumably at the flexible linker region between the N- and C-terminal halves, enabling the N-terminus and the C-terminus to interact with tropomyosin and with nebulin, respectively.

This binding model implies that tropomodulin binding to the pointed end of F-actin is coincident with the interaction with tropomyosin and nebulin. Such multi-site binding would explain the double mechanism for the actin filament length regulation. Generally, the length of the thin filament is stochastically regulated at the pointed end through the pool sizes of free tropomyosin, actin, and tropomodulin (Littlefield et al., 2001), in which the filament length is mainly specified by the position of the tropomyosin molecule at the pointed end. The tropomyosin molecule has the lowest probability of removal from the pointed end, because this molecule interacts with many actin subunits and the adjacent tropomyosin molecule. Even if the stochastic length determining mechanism works without nebulin, like in the embryonic myocytes and cardiac muscle cells, once the nebulin molecules extend to the pointed end, as in adult vertebrate skeletal muscle, the length-determining mechanism dependent on nebulin (Labeit et al., 1991; Trinick, 1994) would go into action. This mechanism does not replace the former one, but rather the two mechanisms may coexist so that the filament length is more finely specified by the position of the N-terminus of nebulin.

We thank Dr. S. Adachi and Dr. S-Y. Park, of RIKEN Harima Institute at SPring-8, for help in data collection at BL44B2; Dr. F. Samatey and Dr. K. Imada of ERATO Project, Seika, Japan, for advice regarding structure determination; Dr. C. C. Gregorio, of the University of Arizona, Tucson, AZ, for the expression plasmids of the N-terminal fragments of nebulin and for discussions; Dr. V. M. Fowler of the Scripps Research Institute, La Jolla, CA, for discussions; and Dr. H. Nakamura, of Osaka University, for discussions on the surface potential of proteins.

This work was supported in part by the Special Coordination Funds for Promoting Science and Technology from the Ministry of Education, Culture, Sports, Science and Technology of the Japanese Government.

REFERENCES

Altschul, S. F., T. L. Madden, A. A. Schaffer, J. Zhang, Z. Zhang, W. Miller, and D. J. Lipman. 1997. Gapped BLAST and PSI-BLAST: a new generation of protein database search programs. *Nucleic Acids Res.* 25:3389–3402.

Babcock, G. G., and V. M. Fowler. 1994. Isoform-specific interaction of tropomodulin with skeletal muscle and erythrocyte tropomyosins. *J. Biol. Chem.* 269:27510–27518.

Brünger, A. T. 1992. X-PLOR Manual Version 3.1. Yale University Press, New Haven, CT.

Buchanan, S. G., and N. J. Gay. 1996. Structural and functional diversity in the leucine-rich repeat family of proteins. *Prog. Biophys. Mol. Biol.* 65:1–44.

CCP4. 1994. The *CCP*4 suite: programs for protein crystallography. *Acta Crystallogr. D.* 50:760–763.

Conley, C. A., K. L. Fritz-Six, A. Almenar-Queralt, and V. M. Fowler. 2001. Leiomodins: larger members of the tropomodulin (tmod) gene family. *Genomics.* 73:127–139.

Cox, P. R., and H. Y. Zoghbi. 2000. Sequencing, expression analysis, and mapping of three unique human tropomodulin genes and their mouse orthologs. *Genomics.* 63:97–107.

Fowler, V. M. 1990. Tropomodulin: a cytoskeletal protein that binds to the end of erythrocyte tropomyosin and inhibits tropomyosin binding to actin. *J. Cell Biol.* 111:471–481.

Fujisawa, T., A. Kostyukova, and Y. Maéda. 2001. The shapes and sizes of two domains of tropomodulin, the P-end-capping protein of actin-tropomyosin. *FEBS Lett.* 498:67–71.

Fujita-Becker, S., L. Kluwe, A. Miegel, K. Maeda, and Y. Maéda. 1993. Reconstitution of rabbit skeletal muscle troponin from the recombinant subunits all expressed in and purified from *E. coli*. *J. Biochem. (Tokyo).* 114:438–444.

Gregorio, C. C., A. Weber, M. Bondad, C. R. Pennise, and V. M. Fowler. 1995. Requirement of pointed-end capping by tropomodulin to maintain actin filament length in embryonic chick cardiac myocytes. *Nature.* 377:83–86.

Holmes, K. C., D. Popp, W. Gebhard, and W. Kabsch. 1990. Atomic model of the actin filament. *Nature.* 347:44–49.

Kabsch, W., H. G. Mannherz, D. Suck, E. F. Pai, and K. C. Holmes. 1990. Atomic structure of the actin:DNase I complex. *Nature.* 347:37–44.

Kajava, A. V. 1998. Structural diversity of leucine-rich repeat proteins. *J. Mol. Biol.* 277:519–527.

Kobe, B., and J. Deisenhofer. 1994. The leucine-rich repeat: a versatile binding motif. *Trends Biochem. Sci.* 19:415–421.

Kobe, B., and J. Deisenhofer. 1995a. Proteins with leucine-rich repeats. *Curr. Opin. Struct. Biol.* 5:409–416.

Kobe, B., and J. Deisenhofer. 1995b. A structural basis of the interactions between leucine-rich repeats and protein ligands. *Nature.* 374:183–186.

Kobe, B., and A. V. Kajava. 2001. The leucine-rich repeat as a protein recognition motif. *Curr. Opin. Struct. Biol.* 11:725–732.

Kostyukova, A., K. Maeda, E. Yamauchi, I. Krieger, and Y. Maéda. 2000. Domain structure of tropomodulin: distinct properties of the N-terminal and C-terminal halves. *Eur. J. Biochem.* 267:6470–6475.

Kostyukova, A., E. Tiktopulo, and Y. Maéda. 2001. Folding properties of functional domains of tropomodulin. *Biophys. J.* 81:345–351.

Kraulis, P. J. 1991. MOLSCRIPT: a program to produce both detailed and schematic plots for protein structures. *J. Appl. Crystallogr.* 24:946–950.

Krieger, I., A. S. Kostyukova, and Y. Maéda. 2001. Crystallization and preliminary characterization of crystals of the C- terminal half fragment of tropomodulin. *Acta Crystallogr. D.* 57:743–744.

Labeit, S., T. Gibson, A. Lakey, K. Leonard, M. Zeviani, P. Knight, J. Wardale, and J. Trinick. 1991. Evidence that nebulin is a protein-ruler in muscle thin filaments. *FEBS Lett.* 282:313–316.

Labeit, S., and B. Kolmerer. 1995. The complete primary structure of human nebulin and its correlation to muscle structure. *J. Mol. Biol.* 248:308–315.

Littlefield, R., A. Almenar-Queralt, and V. M. Fowler. 2001. Actin dynamics at pointed ends regulates thin filament length in striated muscle. *Nat. Cell Biol.* 3:544–551.

Littlefield, R., and V. M. Fowler. 1998. Defining actin filament length in striated muscle: rulers and caps or dynamic stability? *Annu. Rev. Cell. Dev. Biol.* 14:487–525.

Lorenz, M., D. Popp, and K. C. Holmes. 1993. Refinement of the F-actin model against x-ray fiber diffraction data by the use of a directed mutation algorithm. *J. Mol. Biol.* 234:826–836.

Lukoyanova, N., M. S. VanLoock, A. Orlova, V. E. Galkin, K. Wang, and E. H. Egelman. 2002. Each actin subunit has three nebulin binding sites: implications for steric blocking. *Curr. Biol.* 12:383–388.

McElhinny, A. S., B. Kolmerer, V. M. Fowler, S. Labeit, and C. C. Gregorio. 2001. The N-terminal end of nebulin interacts with tropomodulin at the pointed ends of the thin filaments. *J. Biol. Chem.* 276:583–592.

Meritt, E. A., and M. E. P. Murphy. 1994. Raster3D Version 2.0: a program for photorealistic molecular graphics. *Acta Crystallogr. D.* 50:869–873.

Miegel, A., T. Kobayashi, and Y. Maéda. 1992. Isolation, purification and partial characterization of tropomyosin and troponin subunits from the lobster tail muscle. *J. Muscle Res. Cell Motil.* 13:608–618.

Nicholls, A., K. A. Sharp, and B. Honig. 1991. Protein folding and association: insights from the interfacial and thermodynamic properties of hydrocarbons. *Proteins.* 11:281–296.

Otterbein, L. R., P. Graceffa, and R. Dominguez. 2001. The crystal structure of uncomplexed actin in the ADP state. *Science.* 293:708–711.

Otwinowski, Z. M. W. 1997. Processing of x-ray diffraction data collected in oscillation mode. *Methods Enzymol.* 276:307–326.

Papageorgiou, A. C., R. Shapiro, and K. R. Acharya. 1997. Molecular recognition of human angiogenin by placental ribonuclease inhibitor: an x-ray crystallographic study at 2.0 Å resolution. *EMBO J.* 16: 5162–5177.

Park, M., L. E. Yaich, and R. Bodmer. 1998. Mesodermal cell fate decisions in *Drosophila* are under the control of the lineage genes *numb*, *Notch*, and *sanpodo*. *Mech. Dev.* 75:117–126.

Perrakis, A., R. Morris, and V. S. Lamzin. 1999. Automated protein model building combined with iterative structure refinement. *Nat. Struct. Biol.* 6:458–463.

Pfuhl, M., S. J. Winder, M. A. Castiglione Morelli, S. Labeit, and A. Pastore. 1996. Correlation between conformational and binding properties of nebulin repeats. *J. Mol. Biol.* 257:367–384.

Pfuhl, M., S. J. Winder, and A. Pastore. 1994. Nebulin, a helical actin binding protein. *EMBO J.* 13:1782–1789.

Price, S. R., P. R. Evans, and K. Nagai. 1998. Crystal structure of the spliceosomal U2B"-U2A' protein complex bound to a fragment of U2 small nuclear RNA. *Nature.* 394:645–650.

Roussel, A., and C. Cambillau. 1996. TURBO-FRODO Manual. AFMB-CNRS, Marseille, France.

Saeki, K., K. Sutoh, and T. Wakabayashi. 1996. Tropomyosin-binding site(s) on the *Dictyostelium* actin surface as identified by site-directed mutagenesis. *Biochemistry.* 35:14465–14472.

Terwilliger, T. C., and J. Berendzen. 1999. Automated MAD and MIR structure solution. *Acta Crystallogr. D.* 55:849–861.

Trakhanov, S., D. I. Kreimer, S. Parkin, G. F. Ames, and B. Rupp. 1998. Cadmium-induced crystallization of proteins. II. Crystallization of the *Salmonella typhimurium* histidine-binding protein in complex with L-histidine, L-arginine, or L-lysine. *Protein Sci.* 7:600–604.

Trakhanov, S., and F. A. Quiocho. 1995. Influence of divalent cations in protein crystallization. *Protein Sci.* 4:1914–1919.

Trinick, J. 1994. Titin and nebulin: protein rulers in muscle? *Trends Biochem. Sci.* 19:405–409.

Vera, C., A. Sood, K. M. Gao, L. J. Yee, J. J. Lin, and L. A. Sung. 2000. Tropomodulin-binding site mapped to residues 7–14 at the N-terminal heptad repeats of tropomyosin isoform 5. *Arch. Biochem. Biophys.* 378:16–24.

Weber, A., C. R. Pennise, G. G. Babcock, and V. M. Fowler. 1994. Tropomodulin caps the pointed ends of actin filaments. *J. Cell Biol.* 127:1627–1635.

Weber, A., C. R. Pennise, and V. M. Fowler. 1999. Tropomodulin increases the critical concentration of barbed end-capped actin filaments by converting ADP.P(i)-actin to ADP-actin at all pointed filament ends. *J. Biol. Chem.* 274:34637–34645.

Xu, P., K. I. Mitchelhill, B. Kobe, B. E. Kemp, and H. G. Zot. 1997. The myosin-I-binding protein Acan125 binds the SH3 domain and belongs to the superfamily of leucine-rich repeat proteins. *Proc. Natl. Acad. Sci. U.S.A.* 94:3685–3690.